



Self-supporting overhang structures produced by additive manufacturing through electron beam melting

Wadea Ameen^{1,2} · Abdulrahman Al-Ahmari^{1,2} · Muneer Khan Mohammed²

Received: 15 November 2018 / Accepted: 13 June 2019 / Published online: 28 June 2019
© Springer-Verlag London Ltd., part of Springer Nature 2019

Abstract

The aim of this study is to identify the limitations of self-supporting structures and evaluate the deformations associated with overhang structures fabricated without support structures. To achieve these objectives, a series of experiments involving different overhang geometries were designed, fabricated, and evaluated. The formation of defects during the fabrication of overhanging structures is detailed, and the self-supporting limits for different overhangs are established. A segmentation strategy for the support structure addition is proposed and evaluated in different configurations for ledge overhangs to reduce the amount of support structures without affecting the overhang accuracy. Based on the inferences of this study, design rules are proposed for producing overhang structures through electron beam melting. The results identified the self-supporting limits for different overhang geometries. In addition, the proposed segmentation strategy for support generation in ledge overhangs resulted in reduction of support structure materials and post-processing time without any effect on the quality of the fabricated overhang.

Keywords Additive manufacturing · Self-supporting · Overhang structures · Design for additive manufacturing · Electron beam melting · Support structures

1 Introduction and literature review

Electron beam melting (EBM) is a relatively new AM technology based on the powder bed fusion process, wherein an electron beam is used to selectively melt metal powder based on the computer-aided design (CAD) data to produce near-net-shape parts. The EBM technology is used to produce parts for high-performance applications within biomedical [1–3], aerospace [4], and automotive industries. It is more effective with complex parts manufactured in low volumes, where machining and casting would involve too much lead time and wastage of material. However, the manufacture of overhang structures is one of the major challenges faced by AM technologies. The production of overhangs without support

structures through powder bed fusion processes results in distorted objects, mainly because the loose powder is not thermally conductive [5, 6].

To overcome this limitation, support structures are essential, especially in cases where the optimum orientation does not eliminate overhanging features [7–9]. However, the addition of the support structure results in the increase in designing and building time and requires post-processing for the removal of support structures. The removal of the support structure introduces the risk of scarring or damaging the part. Furthermore, support structures built for the EBM process are mostly dense metal, which is difficult to remove requiring additional time and cost [10]. Since EBM is a new technology, there are no design rules for applying the support structures during the fabrication of overhangs. In addition, the commercial software that is used usually generates the support structures without considering the capabilities and the limitations of EBM process.

Recently, some attention has been given to evaluate the production of the overhang structures using EBM. Vayre et al., 2013, evaluated the distortion level of the overhang surfaces in different orientation angles and the effect of adding the support structures. The distance between the start plate and the first layer and the effect of support structure density on the

✉ Wadea Ameen
Wadeaameen@gmail.com

¹ Industrial Engineering Department, King Saud University, Riyadh, Saudi Arabia

² Raytheon Chair for Systems Engineering (RCSE Chair), Advanced Manufacturing Institute, King Saud University, P.O. Box 800, Riyadh 11421, Saudi Arabia

fabricated overhang quality was also identified [11]. Ameen et al., 2018, evaluated the manufacturability of overhanging holes using EBM. The effect of adding the support structures on the accuracy, mechanical properties, and microstructure during the production of overhang holes was identified [6]. Vora et al., 2013, demonstrated new capabilities of the EBM processes to build overhanging structures without support structures by using the blended powder approach. Al–Si and Ti64–Cu alloy systems were successfully processed, and support-free overhang structures of 5-mm dimension were produced without any warping or distortion [12]. Cloots et al. developed a segmentation strategy for assigning support structures for selective laser melting parts. In the developed strategy, overhanging structures and surfaces were classified as uncritical regions when the overhanging region is surrounded with a sufficient solid material to dissipate the heat and as critical where no sufficient measures for heat dissipation are unavailable [13]. Some attention has been given to develop a simulation model for modeling the AM process [14–16]. To simulate the temperature and stress fields while building a Ti-6Al-4V simple overhang through EBM and examine the root cause of overhang warping, Cheng et al., 2014, developed a three-dimensional (3D) finite element (FE) thermomechanical model. It was found that the poor thermal conductivity of the powder material resulted in higher temperatures and slower heat dissipation in the overhang part [17]. Cheng and Chou, 2014, developed a two-dimensional (2D) FE model to simulate the thermomechanical process and evaluate the effect of the EBM process parameters on the severity of thermal stresses during the manufacture of overhang parts. It was found that for a uniform set of process parameters, the overhang areas have a higher maximum temperature, higher tensile stress, and a larger distortion than the areas on a solid substrate. In addition, a higher energy density may cause more severe curling at the overhang area [17]. Cheng and Kevin, 2015, developed a 2D thermomechanical FE model to simulate the deformation (warping) on different overhang supports in the EBM process. In this model, the effects of process parameter, overhang, support structure, and powder porosity

on overhang deformations were evaluated [18]. Cheng et al., 2014, developed a 3D FE thermomechanical model for temperature and stress simulations in EBM. The temperature and stress distributions during the fabrication of Ti-6Al-4V overhang features were investigated to measure overhang warping [10]. Chou et al., 2014, proposed systems and methods for designing and fabricating contact-free support structures for overhang surfaces using EBM, wherein one or more unmelted powder layers are disposed in a gap between a lower surface of the overhang surface and an upper horizontal surface of the support structure. Heat is conducted from the overhang surface to the support structure through the unmelted powder. The support structure acts as heat sink, thereby enhancing heat transfer and reducing the temperature and severe thermal gradients, which arise owing to the poor thermal conductivity of the powder underneath the overhang [19]. Rami and Frederic proposed a methodology for the design and optimization of support structures in the EBM process. New support structures were designed and their efficiencies were studied. The results showed a reduction in geometric defects [20]. Cheng et al., 2017, developed a general framework for the design and optimization of the overhang support structure by using a 3D thermomechanical FE model for the EBM process. The support structure design problem was formulated using the combined minimum energy and effective heat dissipation methods. The developed FE model was then used to identify the locations where a support anchor was required and determine the support material usage [21]. From the literature review, it is clear that there is a limited research on the fabrication of overhang structures by using EBM. Also, there are no specific design rules for support structure generations during the fabrication of overhangs in EBM.

In this study, the deformations associated with overhang structures fabricated without support structures are evaluated and the limitations of self-supporting overhang structures are identified. In addition, a methodology is developed for designing the appropriate support structures that result in parts free from deformations while consuming minimum time and material.

Fig. 1 Fundamental overhang structures (adapted from [22])

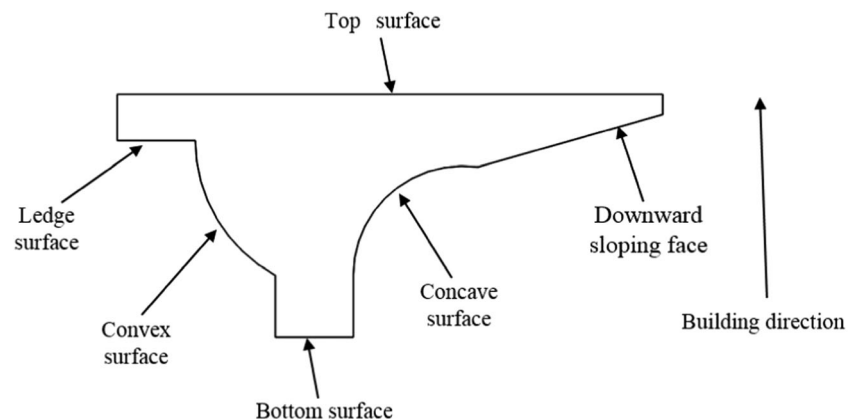
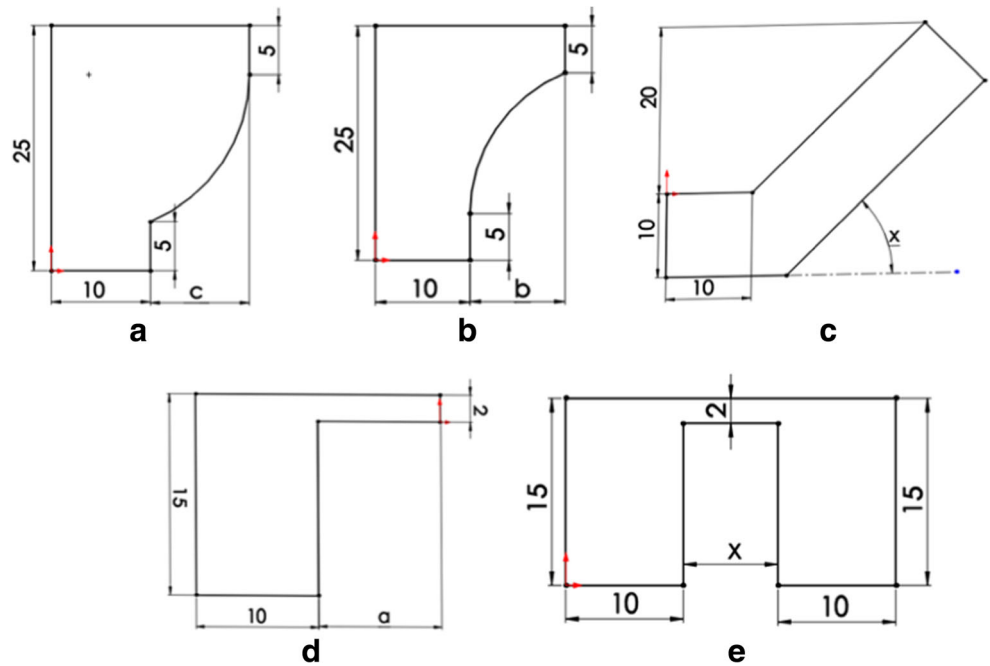


Fig. 2 Overhang structures. **a** Convex radii ($c = 3\text{--}15$ mm, increment of 1 mm). **b** Concave radii ($b = 3\text{--}15$ mm, increment of 1 mm). **c** Slope overhang ($x = 20^\circ\text{--}60^\circ$, increment of 5°). **d** Ledge surface ($a = 1\text{--}15$ mm, increment of 1 mm). **e** Bridge overhang ($x = 1\text{--}10$ mm, increment of 1 mm)



2 Experimental procedures

2.1 Overhanging structures design

An overhanging structure is a part of a component that is not supported by a solidified material or substrate during the fabrication process. Figure 1 shows the fundamental overhang structure geometries that include convex radii, concave radii, downward sloping face, and ledge surfaces.

To identify the self-supporting limitations and evaluate the deformations associated with the fabrication of overhang structures without support structures, five overhang structures were designed, fabricated, and evaluated, as shown in Fig. 2. The overhang structure dimensions were chosen according to

the published scientific works [5, 10, 12, 20, 23–25]. The thickness of overhanging portion of the ledge structure was maintained at approximately 2 mm to make the deformation visible and to avoid potential damage to the machine rake in case of warping [20]. All the test specimens were supported with 4-mm height block support structures only at the bottom surface to prevent any movement of the part during the fabrication process. No support was applied for the overhang portion.

The effect of the solid support dimensions (L, H) and the overhang portion dimensions (T, W) on the quality of the ledge overhang structure is investigated through the design, fabrication, and evaluation at different levels of each dimension, as shown in Fig. 3. The selected dimensions and their respective levels are listed in Table 1.

To reduce the amount of support structures used for the fabrication of ledge overhangs, the segmentation strategy is implemented in different configurations and in different directions, as shown in Fig. 4.

Table 2 lists the chosen levels for each segmentation direction. More levels are considered for segmentation direction “d” due to its expected promised results.

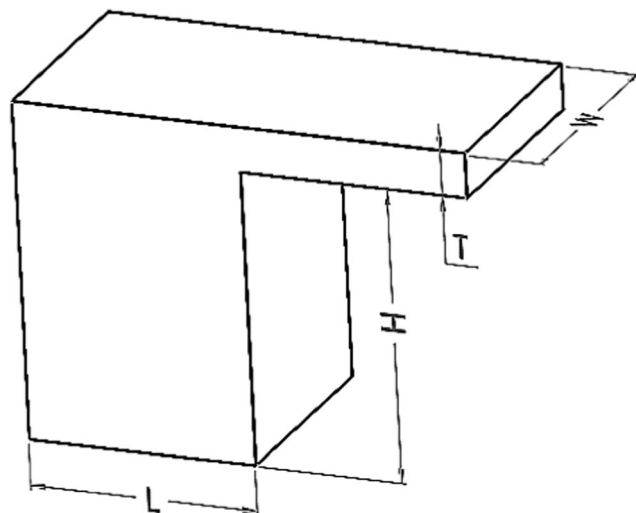


Fig. 3 Ledge overhang structure dimensions

Table 1 Dimensions and their selected levels

Variables (mm)	Level 1	Level 2	Level 3
T	1	2	3
W	5	10	15
L	3	5	10
H	3	8	10

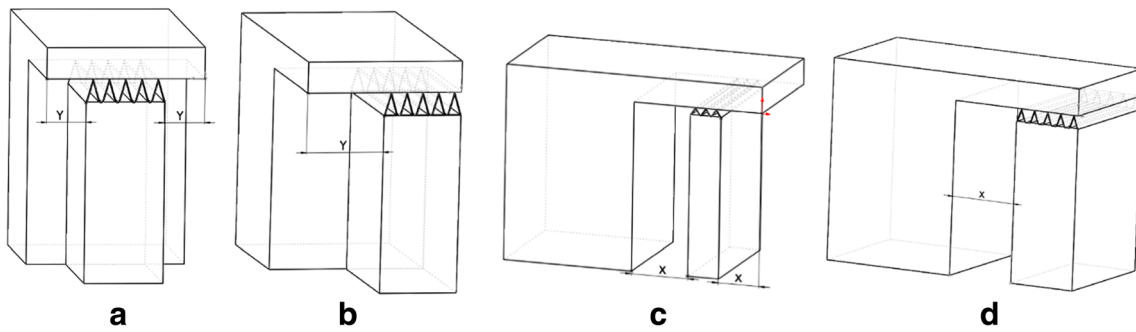


Fig. 4 Support structures segmentation directions. **a** One-side segmentation $Y = 20, 40, 60, 80$ mm. **b** Two-side segmentation $Y = 20, 40, 60, 80$ mm. **c** x from 10 to 90 mm, with an increment of 10 mm. **d** Two x segmentation, $x = 10, 20, 30$ mm

Table 2 Segmentation directions and their selected levels

Segmentation method	1	2	3	4	5	6	7	8	9
a	20	40	60	80	–	–	–	–	–
b	20	40	60	80	–	–	–	–	–
c	10	5	10	–	–	–	–	–	–
d	10	20	30	40	50	60	70	80	90

2.2 Experimental material and equipment

Titanium alloy (Ti6Al4V) powder with the chemical composition as shown in Fig. 5 (energy-dispersive X-ray (EDX) test result) is used as the feedstock material. The particle size analysis revealed the size of powder particles to be in the range 49–103 μm , with a mean of around 71 μm as shown in Fig. 6. The morphology of the powder was mostly spherical, with some smaller particles adhering to the bigger ones. Figure 7 shows the scanning electron microscope (SEM) analysis of titanium alloy extra low interstitials (Ti6Al4V ELI) powder.

ARCAM A2, an EBM setup from ARCAM AB, Mölndal, Sweden, was used to fabricate the test parts with default process parameters as listed in Table 3. In this process, an electron beam melts the metal alloy powder into a fully solid part in a layer-by-layer manner. The schematic diagram of this process is shown in Fig. 8; the electrons are emitted from the tungsten

filament, which is heated at above 2500 $^{\circ}\text{C}$. These high-energy electrons are accelerated through the anode. The magnetic field of lenses brings the beam into focus and electromagnetically scanned. When the high-energy electrons hit the titanium powder, their kinetic energy is transformed into heat energy, which then melts the powder. The titanium powder is fed by gravity from cassettes and is raked into layers across the table. The built specimen is lowered on to the built table with each layer melt cycle until the completion of build. In the current work, the layer thickness is set as 0.05 mm (compatible with available process parameter theme and it is the minimum layer thickness for EBM). All the process is performed under vacuum, which eliminates impurities and yields high strength properties of the material. Once the build is finished, the parts are then cooled to room temperature within the machine chamber.

The fabricated parts are then subjected to the powder recovery system (PRS) to blast the sintered powder using compressed air. Figure 9 shows samples of the fabricated specimens after removing the bonded powder.

To investigate the quality of the fabricated specimens, various tests are carried out such as visual inspection, measurement using a white light microscope (Mikroskop Technik Rathenow) in combination with a DSLR camera (Canon EOS 600D), and, finally, mechanical property and microstructural evaluations.

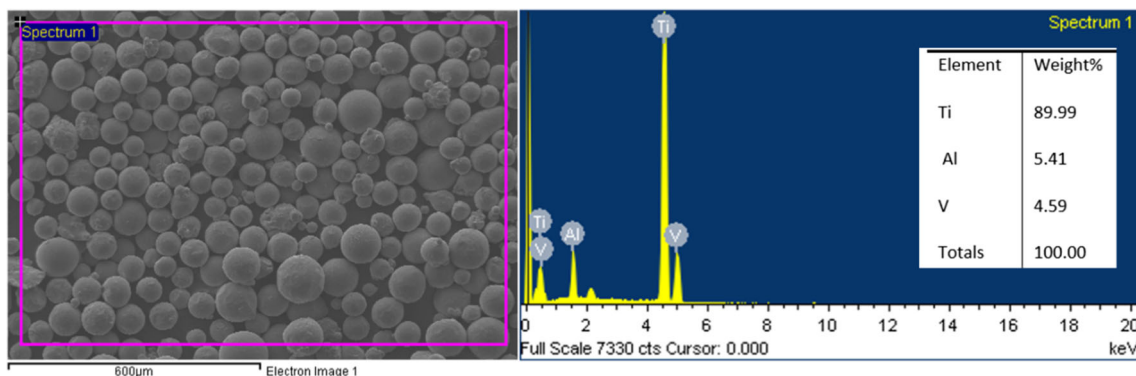


Fig. 5 Chemical composition of Ti6Al4V ELI powder

Fig. 6 Powder particle size distribution measured through laser diffraction technique

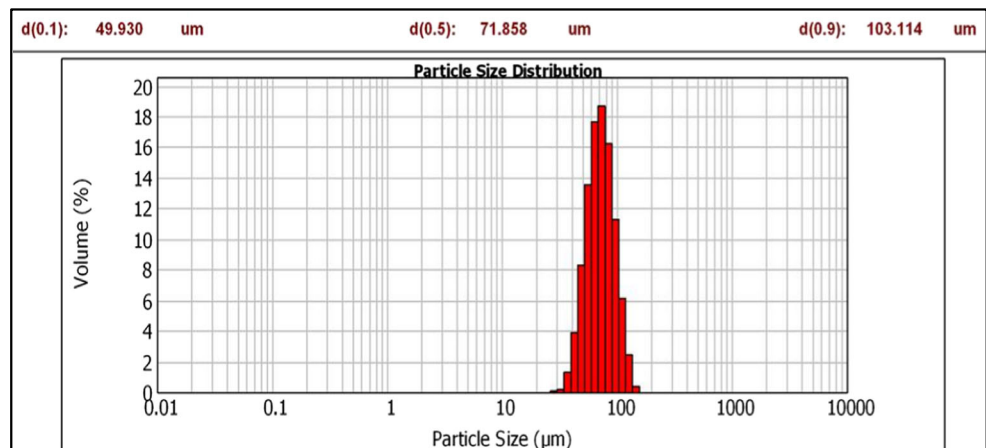
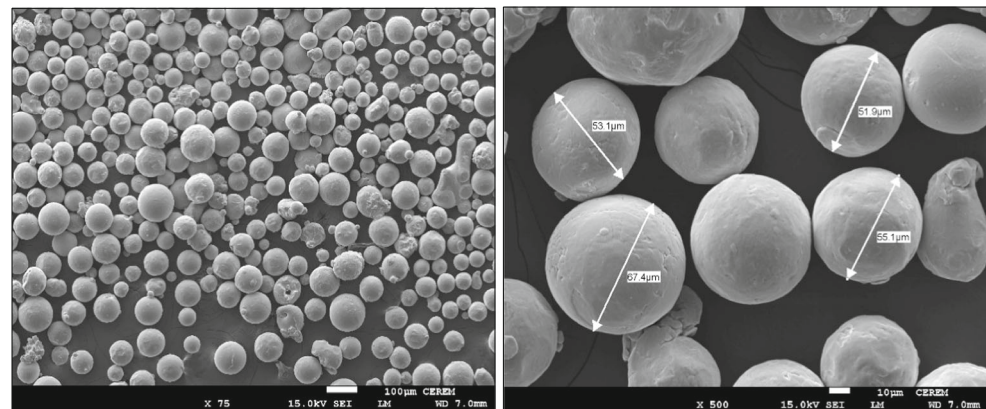


Fig. 7 Scanning electron microscope image of Ti6Al4V ELI powder particles



To measure the deformation, the test specimen is placed under the microscope along with the test part drawing printed on 90-gsm semitransparent paper. After the appropriate alignment, the part is compared against the original geometry with the help of the semitransparent paper, including the part number as shown in Fig. 10. Three samples each of all overhang structure specimens were measured and then their averages were computed.

The mechanical properties play an important role in actual applications; as it is difficult to conduct a tensile test on small

size samples (overhang structures), micro Vickers hardness values are used to estimate the yield strength of the fabricated overhang structures by using the relation ($\sigma_y \approx HV/3$) [4, 6, 26]. ZHVµ micro Vickers hardness from Zwick/Roell with 10-s dwell time and 500-gf force is used for the hardness test.

To study the effect of the support structure on the mechanical properties, the samples are ground and polished for the hardness test. The tests are conducted near the bottom edge of the overhangs, as shown in Fig. 11. Multiple hardness measurements are taken along the edge, and then the averages are calculated. For the microstructural analysis, polished specimens are etched for 10 s using a modified Kroll’s reagent (2 ml hydrofluoric acid, 6 ml nitric acid, and 92 ml distilled water).

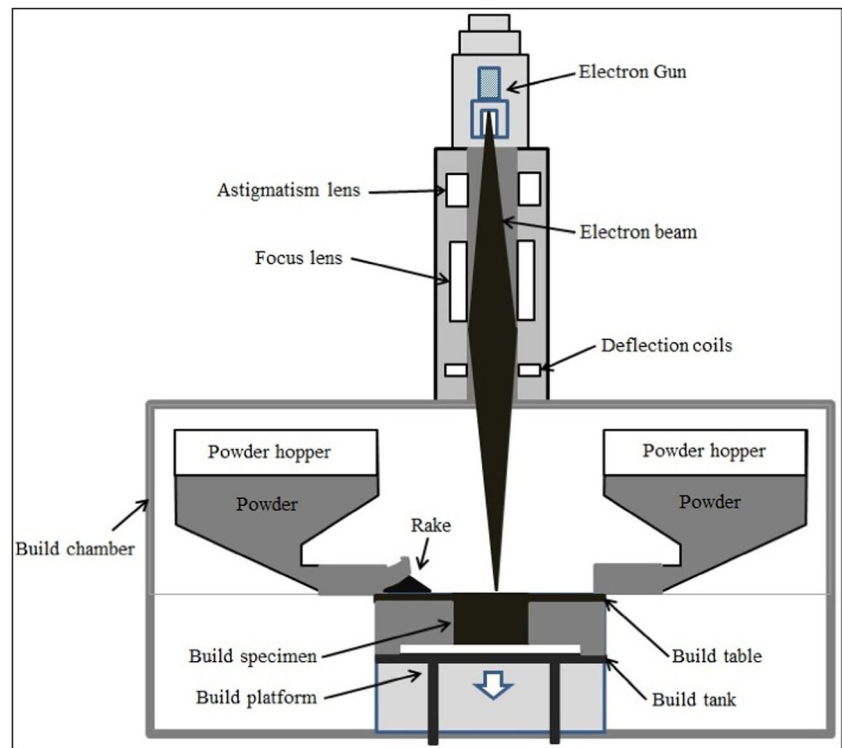
Table 3 Default EBM process parameters

Parameters	Values
Beam current, I_b (mA)	15
Scan speed, v (mm/s)	4530
Focus offset (mA)	3
Line offset (mm)	0.1
Acceleration voltage, U (kV)	60
Electron beam diameter, Φ (µm)	200
Powder layer thickness (mm)	0.05
Beam penetration depth, dP	1.5 layer
Preheat temperature, $T_{preheat}$ (°C)	750

3 Analysis of results

All the test specimens were successfully fabricated using EBM without any harm/damage to the machine (i.e., the teeth of the machine rack). Some of the specimens fabricated without support structures showed significant deformations, which was overcome by the flexibility of the machine rake. From the visual inspection, it is clear that EBM is capable of fabricating some overhang structures

Fig. 8 Schematic diagram of electron beam melting process



successfully without support structures; however, the process has limitation in respect of some overhang structures. For the purpose of comparison between the results of the present study and the default support structures from the Magics® software, the support structures are generated automatically for some overhangs, as shown in Fig. 12.

The concave and convex overhangs are self-supporting for the 4-mm radius and 65° angle overhangs. There is no self-supporting limit in the case of specimens where the overhang portions are parallel to the base plate like the ledge overhangs, whereas the 1-mm bridge overhangs are self-supporting. The following sections will evaluate and identify the self-

Fig. 9 Fabricated specimens. **a** Concave radii. **b** Convex radii. **c** Slope overhang. **d** Ledge overhang

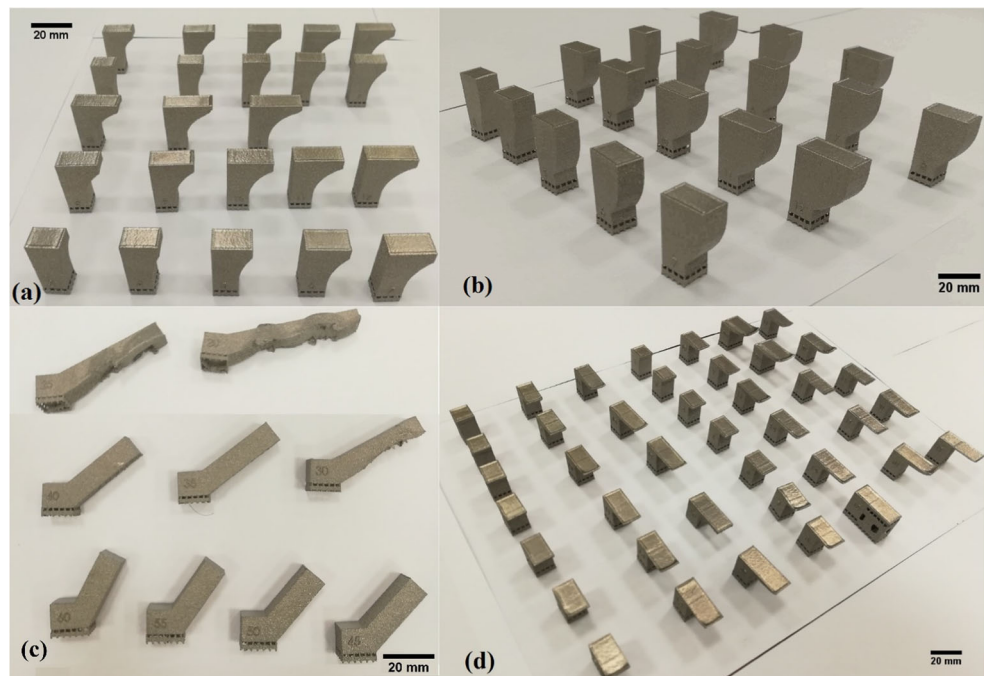
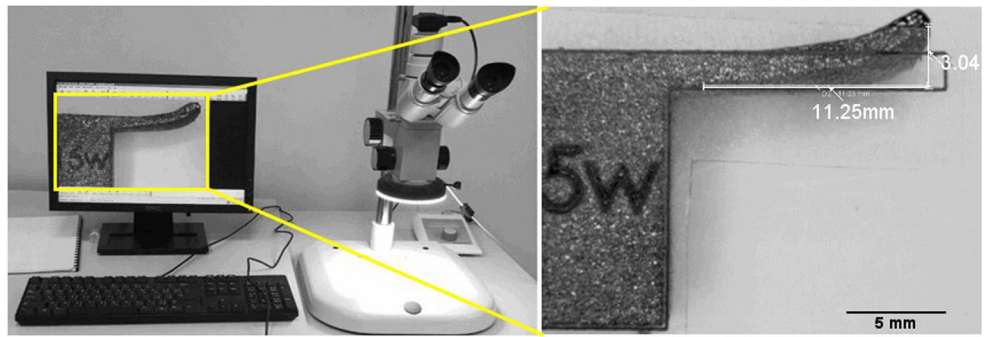


Fig. 10 Warping deformation measurement by using Mikroskop Technik Rathenow



supporting limits and the associated deformations of the different overhangs built without supports.

3.1 Overhang deformations and self-supporting limitations

3.1.1 Convex overhang

Initially, convex overhang specimens were examined through visual inspection. These initial observations confirmed the effectiveness of EBM to fabricate convex overhang structures without support structures. The overhangs were free from defects up to a certain limit, after which there was some deformation. Figure 13 shows the effect of the support structure addition to the convex overhang having a radius more than the self-supporting limit.

The evaluation of convex overhang structures by using the microscope indicated the 7-mm convex radius as the self-supporting limit for the EBM to fabricate defect-free specimens without support structures. The results also showed that unsupported fabrication of convex overhangs of a radius more than 7 mm resulted in shape distortion due to loss of material on the overhanging surface. This deformation increases with an increase in the convex radius, as shown in Fig. 14. The fabricated overhangs held its convex shape until the 12-mm radius on the side surfaces but they were associated with multiple inaccuracies as shown in Fig. 15. The actual radius of the convex overhang was not same as the radius of computer-aided design (CAD) models. The surface quality near the lower region of the convex radius was found to be poor as compared to other regions due to the loss of material defect.

The results obtained in this study were compared with the default support structures generated by Magics® software. It can be seen in Fig. 12 that the default self-supporting limit in the Magics® software for the convex overhangs is 4-mm radius, whereas in this study it was found that the self-supporting limit for EBM to fabricate defect-free convex overhangs is 7 mm. These results show that the commercial software sometimes generates nonessential support structures, which results in the increase in

material consumption, build time, and post-processing time.

3.1.2 Concave overhang

Two main defects were observed in concave overhang structures fabricated without supports. One was the bottom edge defect of the overhang (none of the overhanging ends achieved rectangular geometry) and the other was the warping in upper layers of the overhang as shown in Fig. 16. The level of warping deformation appeared to become a reliable visual representation that occurred during the build. The microscopic images showed the self-supporting limit of the 8-mm radius for the concave overhang produced without support and free from defects as shown in Fig. 17. The self-supporting limit is relatively wide in the concave overhang; this is because of the shape of the overhang in which each layer is supported by the previous one. In addition, visual inspection showed the surface quality on the concave radius degraded as radius increased. Similar to the convex overhangs, the default self-supporting limit for the concave overhangs is 4-mm

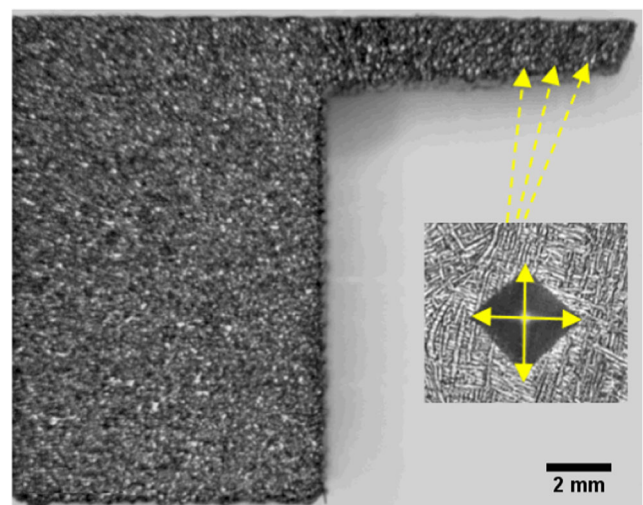


Fig. 11 Microhardness test locations

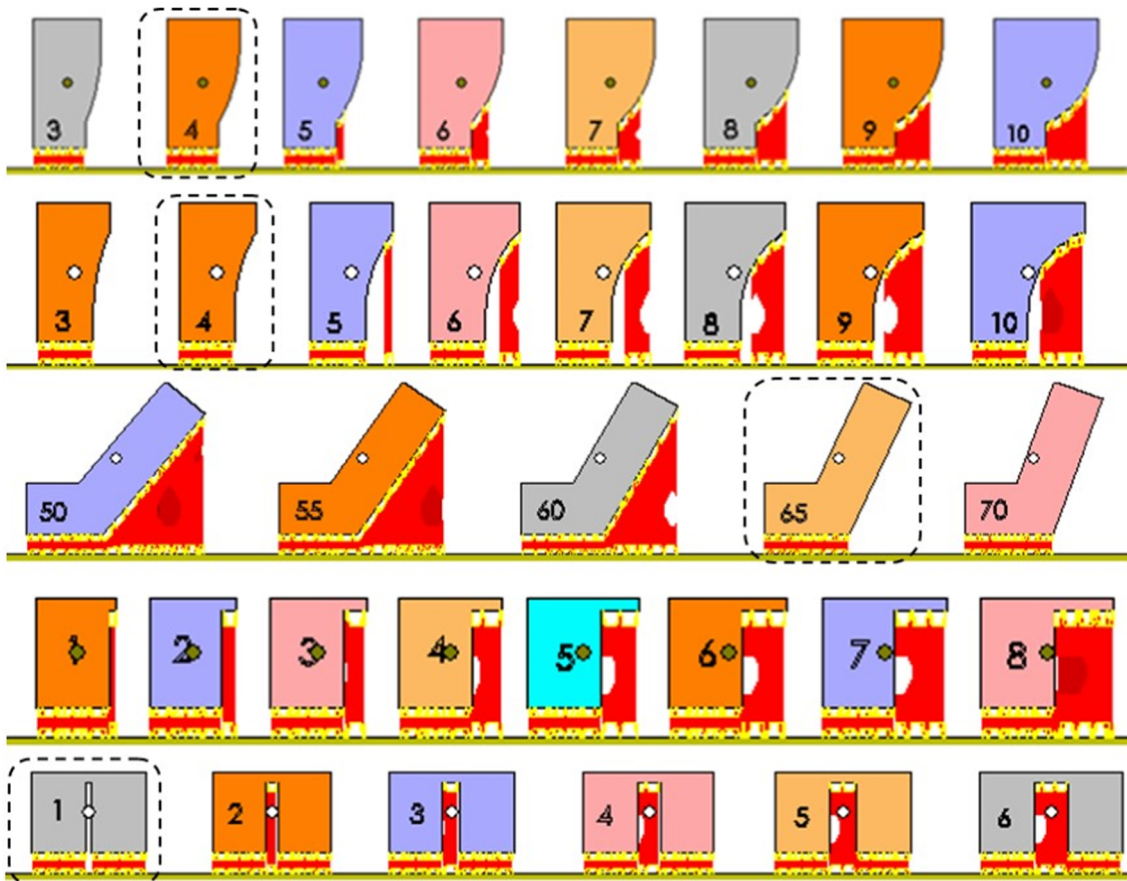


Fig. 12 Magics default support structures for overhang structures

radius in the Magics® software as shown in Fig. 12. It is clear that the commercial software sometimes generates nonessential support structures, which result in an increase in material consumption, build time, and post-processing time. Figure 18 shows the variation in deformation as a function of the concave overhang radius. The deformation increases with an increase in the concave overhang radius.

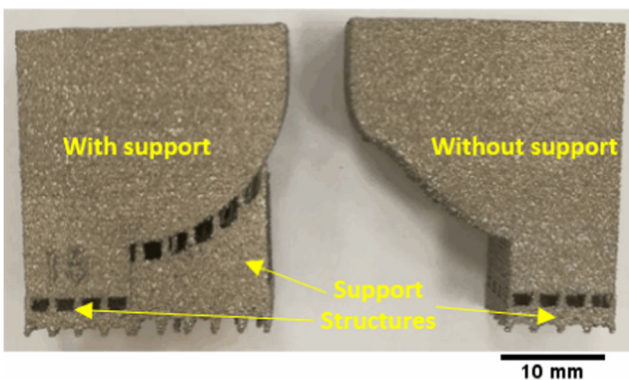


Fig. 13 Convex overhang structures fabricated with and without supports

3.1.3 Slope overhang

The evaluation of slope overhang structures fabricated without supports showed that the minimum angle (critical

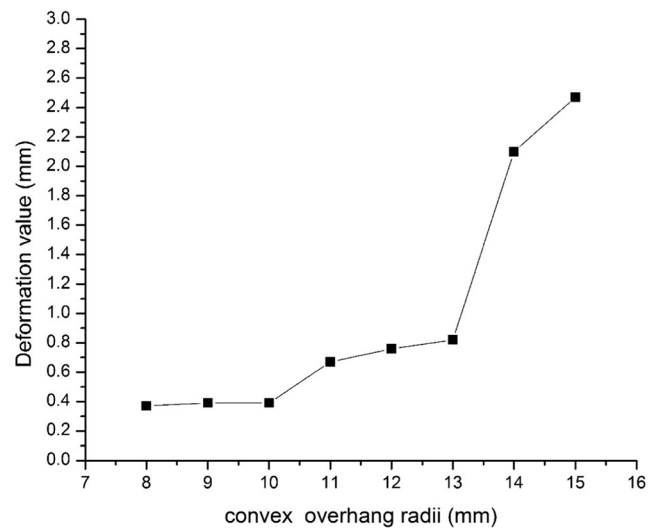


Fig. 14 Overhang deformation as a function of convex overhang radius

Fig. 15 Defective convex overhang structure

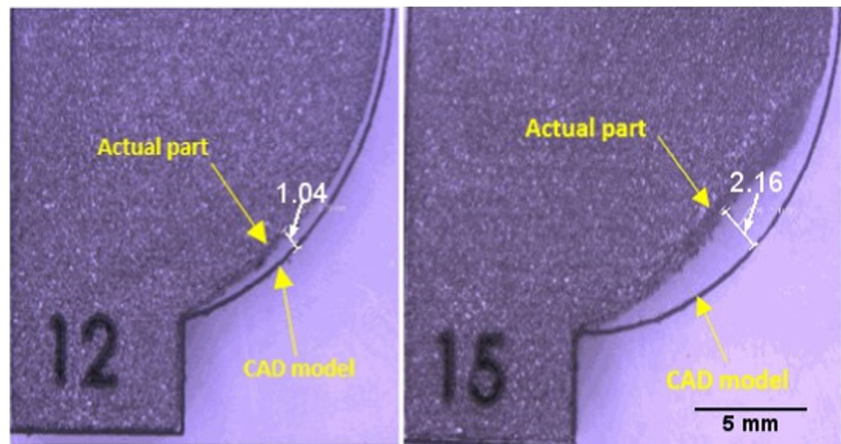
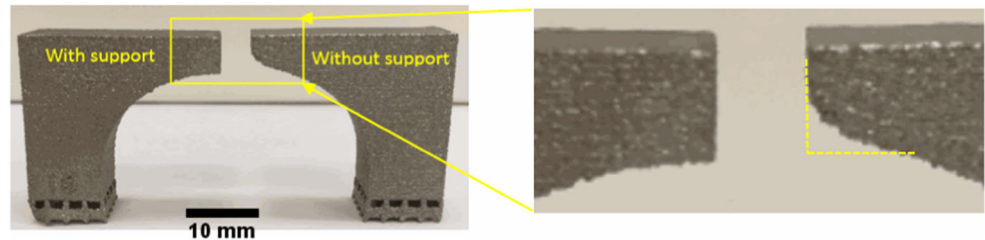


Fig. 16 Concave overhang structures (15-mm radius) with and without support structures



inclined angle) for the defect-free overhang that could be fabricated through EBM is 50°. Therefore, the 50° angle is considered the self-supporting limit for fabricating slope overhang structures using EBM. The production of slope overhangs with angles less than 50° and greater than 30° resulted in loss of material and curved bottom surfaces without any deformation on the edges of the overhang, as shown in Fig. 19. The fabrication of slope overhangs with angle equal or less than 30° resulted in dross formation and edge loss owing to the unstable melt pool at the bottom. In addition, the surface quality on the downward faces of the slope overhangs deteriorated as overhang angle decrease. The default limit for slope overhangs to be produced without support by EBM using Magics® software is 65° slope as shown in the Fig. 12. However, in this study, it was found that EBM could fabricate defect-free overhangs without support up to 50° slope.

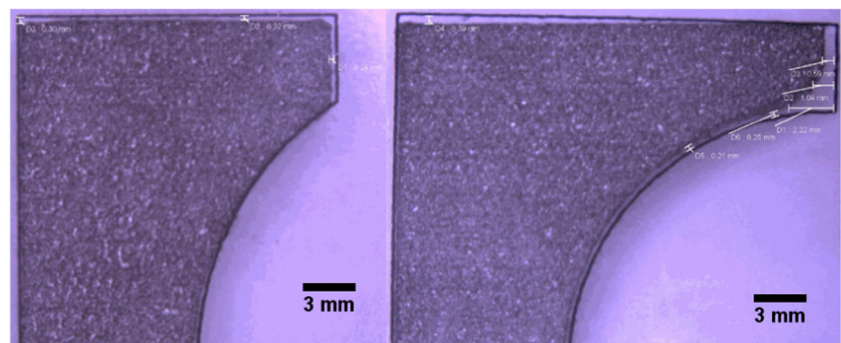
3.1.4 Bridge overhang support

A bridge overhang structure is similar to a ledge overhang wherein the overhang portion is parallel to the base plate. However, in the bridge overhang, the layers of the overhang portion are built between two solid supports that facilitate the fabrication of this overhang without support structure up to a certain limit. The results showed that EBM is useful to fabricate defect-free bridge overhangs without support structures up to 5-mm length, beyond which any increase in the overhang length results in warping deformation in the middle of the overhang, as shown in Fig. 20.

3.1.5 Ledge overhang

The evaluation of the self-supporting limit for the ledge overhang shows that the addition of support structure is necessary, wherein the overhang length is 1 mm. Fabrication of ledge

Fig. 17 Results of concave overhang structure (8- and 15-mm radii) without support structures



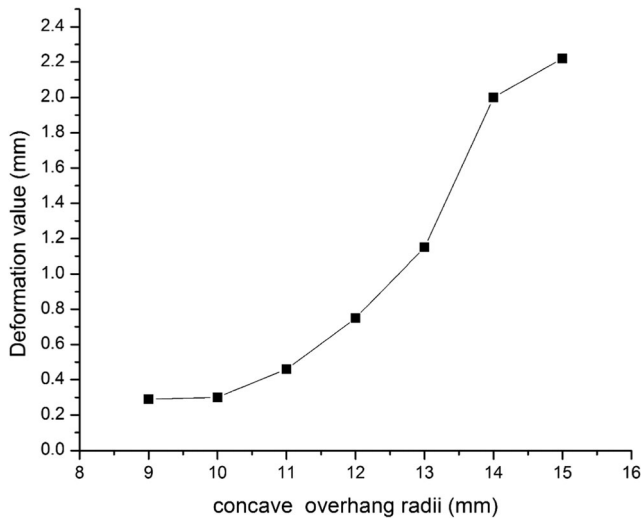


Fig. 18 Concave overhang deformation value as a function of overhang radius

overhangs without support structure resulted in several deformations. The main deformations that were observed are warping, variation in the thickness of the overhang, and vertical side loss as shown in Fig. 21.

The warping distortion was found to have the most significant effect on the part geometry. Two components are

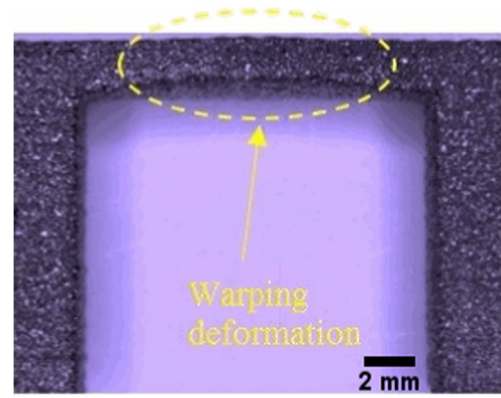
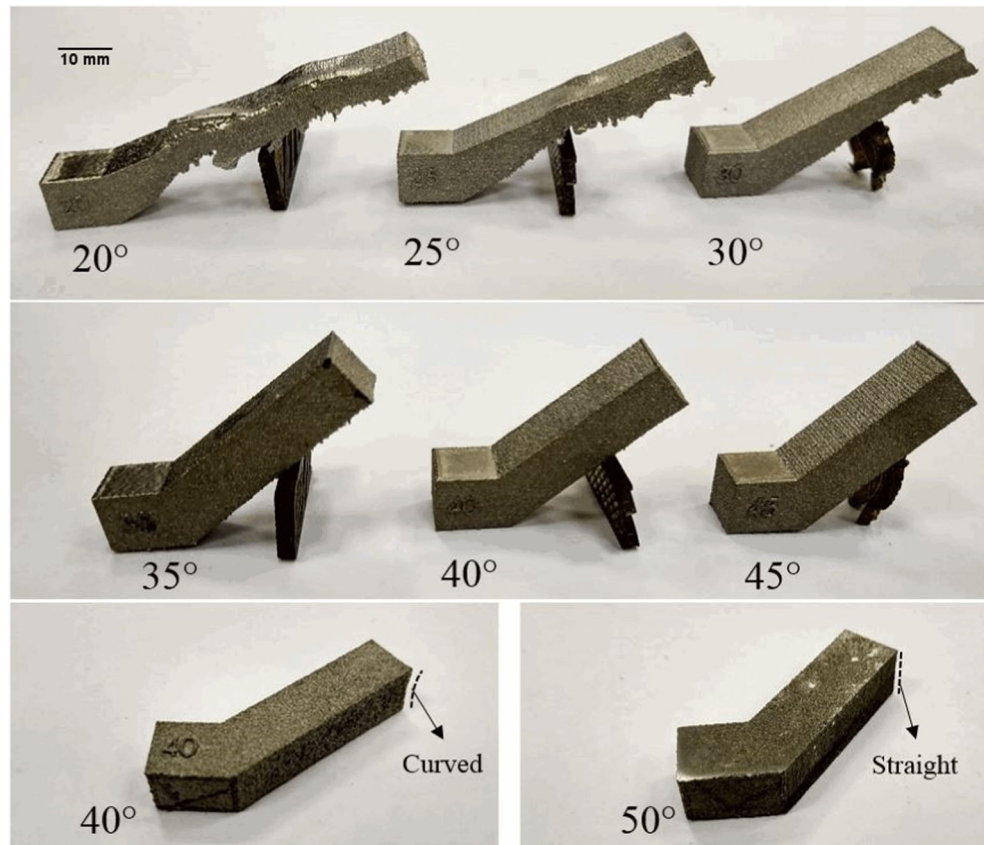


Fig. 20 Deformation in bridge overhang of 15-mm length

considered to evaluate the warping distortion on the ledge overhang, and height and length of the warp, as shown in Fig. 22.

The results showed that it is not possible to fabricate a surface parallel to the build platform unless supports are used. It is found that in general, the warp distortion increases with an increase in the length of the overhang. The increase in warping is significant after 10-mm overhang length; it then peaks at 12 mm and after that, it starts to decrease as shown in Fig. 23.

Fig. 19 Deformation in slope overhang



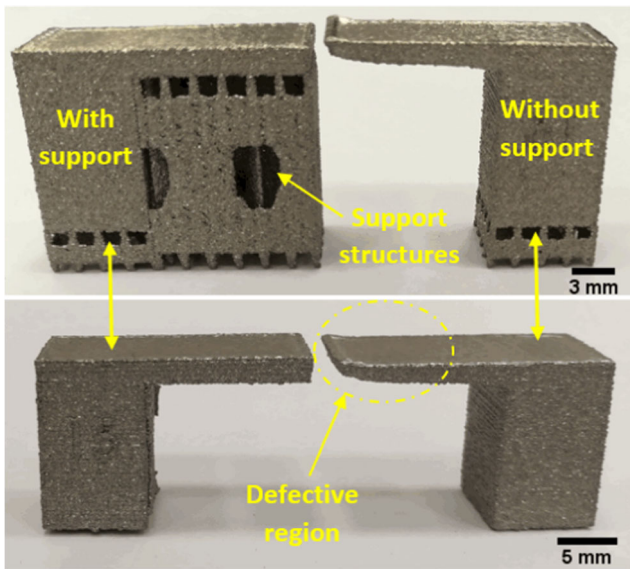


Fig. 21 Deformations in ledge overhang structure

3.2 Effect of ledge overhang dimensions on deformation

To find the effect of ledge overhang dimensions on the resultant deformations, four parameters with three levels each are considered, as listed in Table 1. The results show that, in general, only some of the ledge overhang dimensions have an effect on the amount of deformation.

Ledge overhangs were built with varying thickness and width of the overhanging portion as shown in Fig. 24. It was found that increasing the overhang portion thickness (T) and width (W) resulted in an increase in the overhang warping deformation, as shown in Fig.

Fig. 22 Ledge overhang structure warping deformation

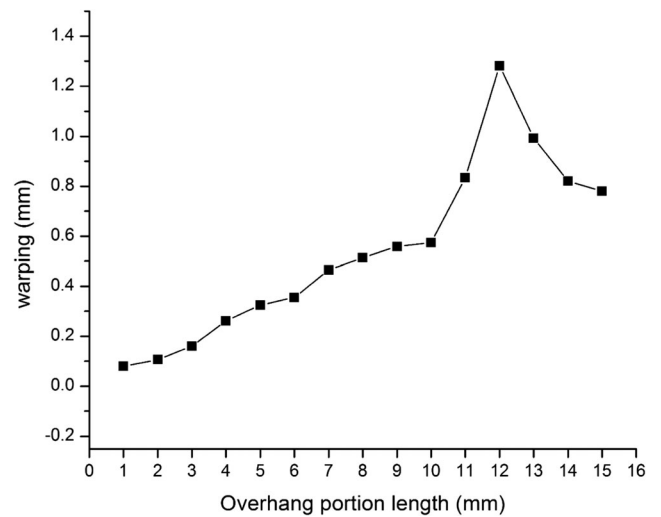
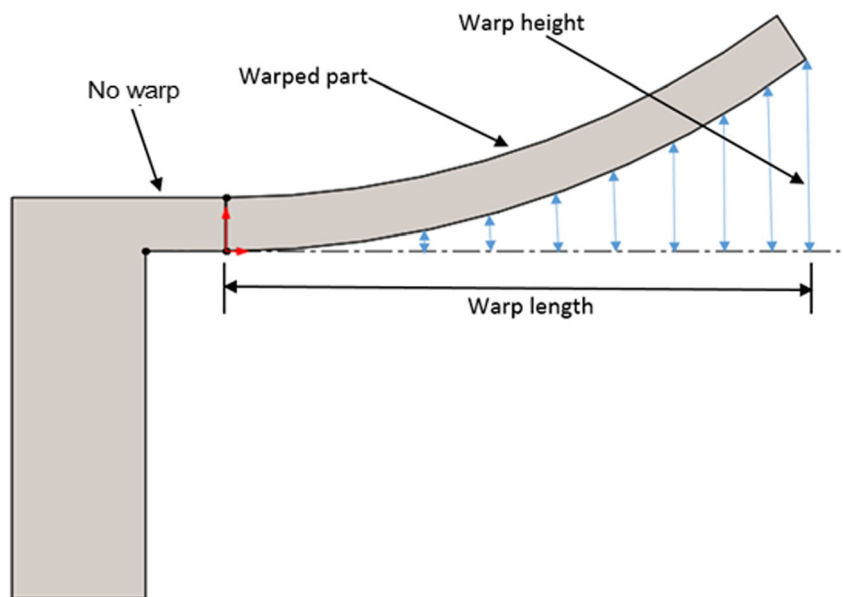


Fig. 23 Effect of overhang portion length on warping

25. This is mainly caused by variations in the number of thermal cycles, higher thermal energy concentrations, and rapid cooling compared to a smaller overhang of the same specimen.

To study the effect of solid support dimensions on the deformations, ledge overhangs were built with varying solid support length and height as shown in Fig. 26. The results show that the solid support length (L) has no effect on warping. However, the warping deformation decreases with an increase in the solid support height (H) in the selected range, as shown in Fig. 27. This is because the overhangs with small solid support height are very close to the baseplate and hence they get more heat from the baseplate. This increase in the thermal energy results in higher warping deformation.

Fig. 24 Variation in deformation versus the thickness and width of ledge overhang

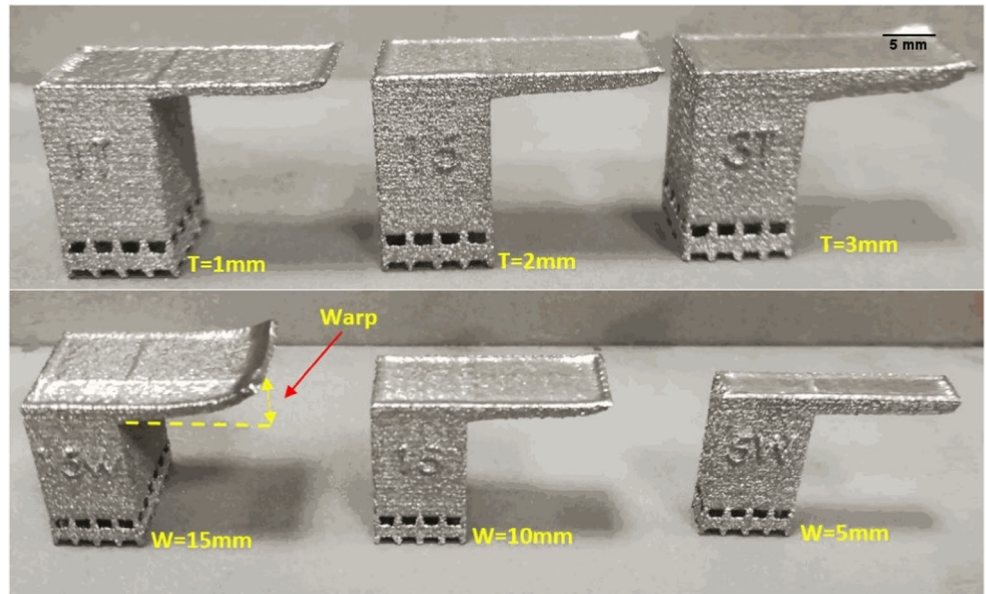
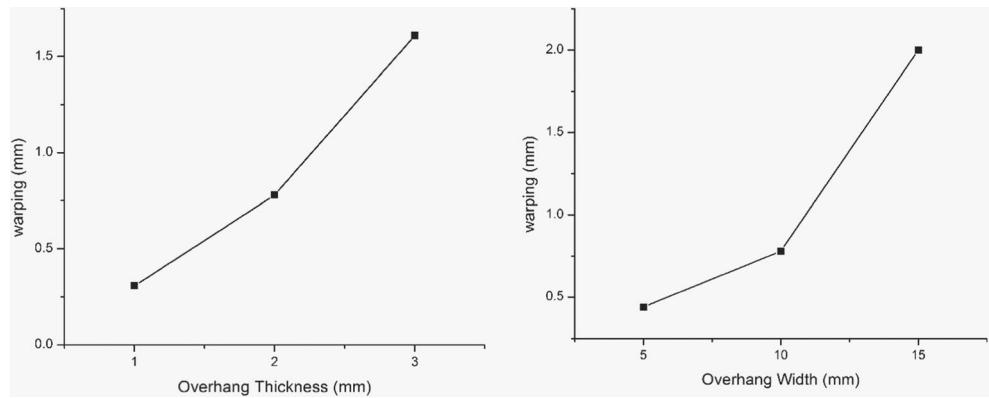


Fig. 25 Effects of thickness and width of overhang portion on warping



3.3 Segmentation strategy for ledge overhang support structures

The segmentation strategy was used for the application of support structures in ledge overhangs. The results showed a

variation in the location and magnitude of warping based on the segmentation direction and dimension.

The application of the support structure with the segmentation strategy on both sides in the Y-direction, as shown in Fig. 4a, resulted in warping near the extreme

Fig. 26 Ledge overhangs with varying solid support length and height

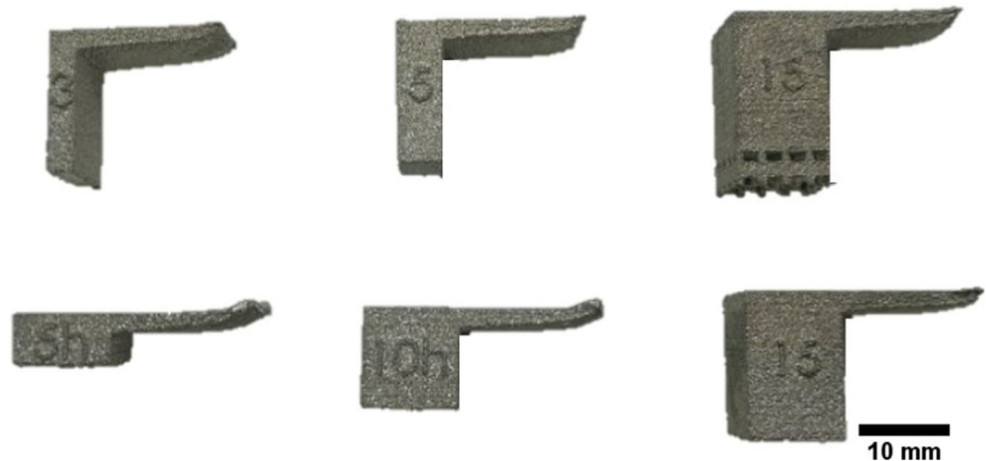


Fig. 27 Effects of the solid support length (L) and height (H) on warping

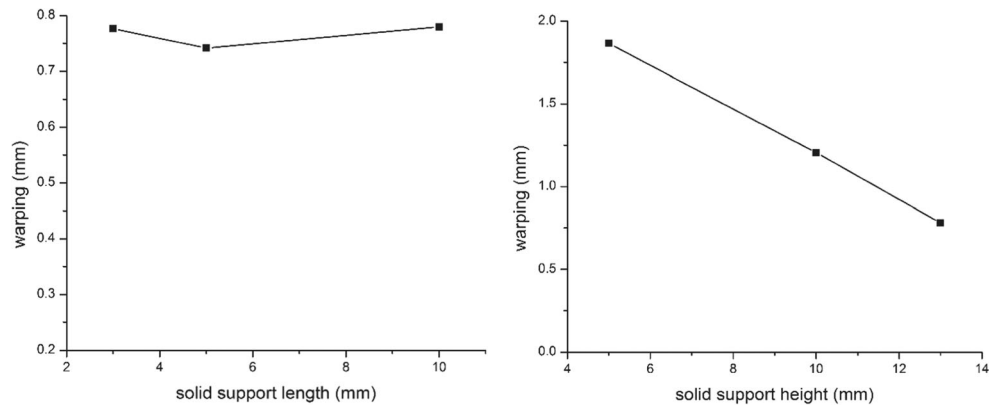


Fig. 28 Segmentation strategy in Y -direction. **a** Two sides. **b** One side

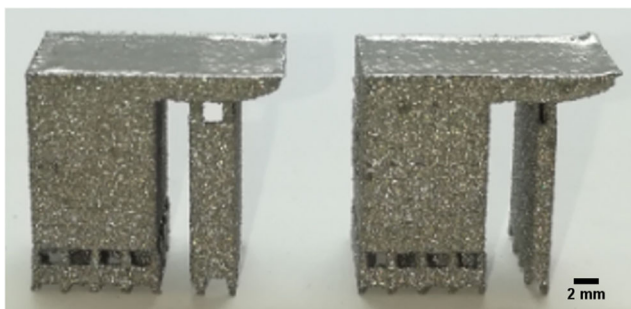
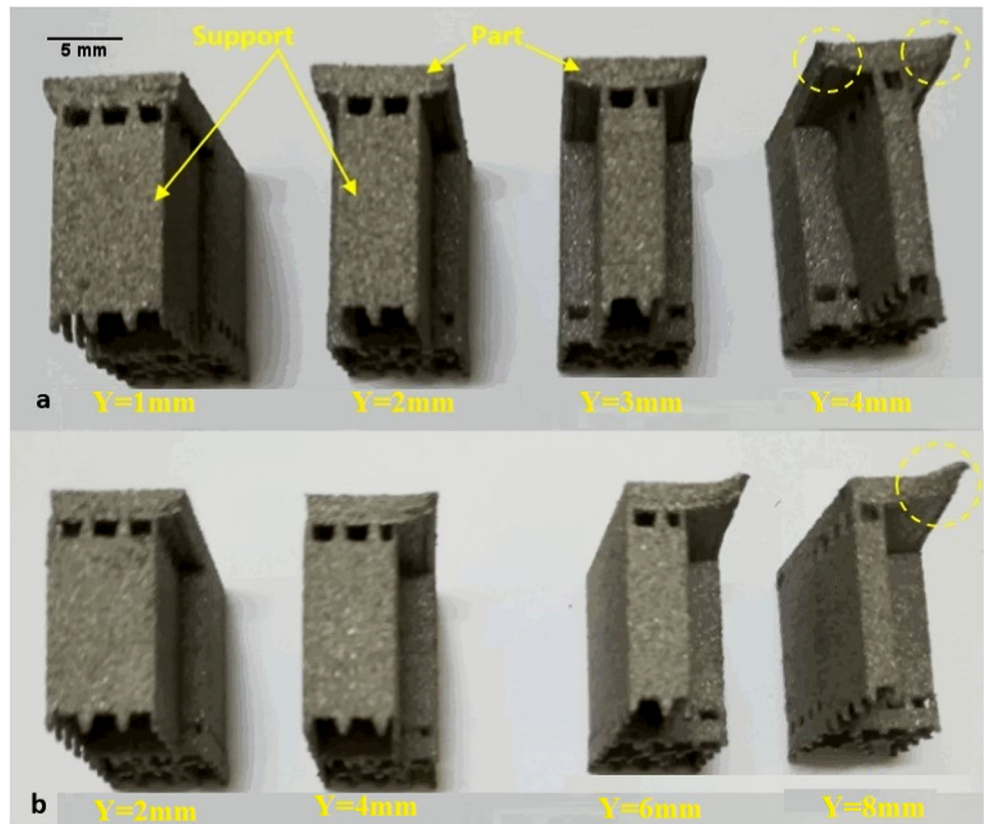


Fig. 29 Segmentation strategy in the middle of the overhang in X -direction

edges of the overhang portion. Increasing the segmentation dimension resulted in an increase in warping deformation near the edges of the overhang portion, as shown in Fig. 28a. Applying the segmentation strategy in the Y -direction on the one side, as shown in Fig. 4b, with varying segmentation dimension resulted in warping deformation at the extreme edge of the overhang portion where the segmentation is applied, and the value of warping increases with an increase in the segmentation dimension, as shown in Fig. 28b. In general, the application of the segmentation strategy in the Y -direction in one or two sides with varying dimensions did not have any positive affect.

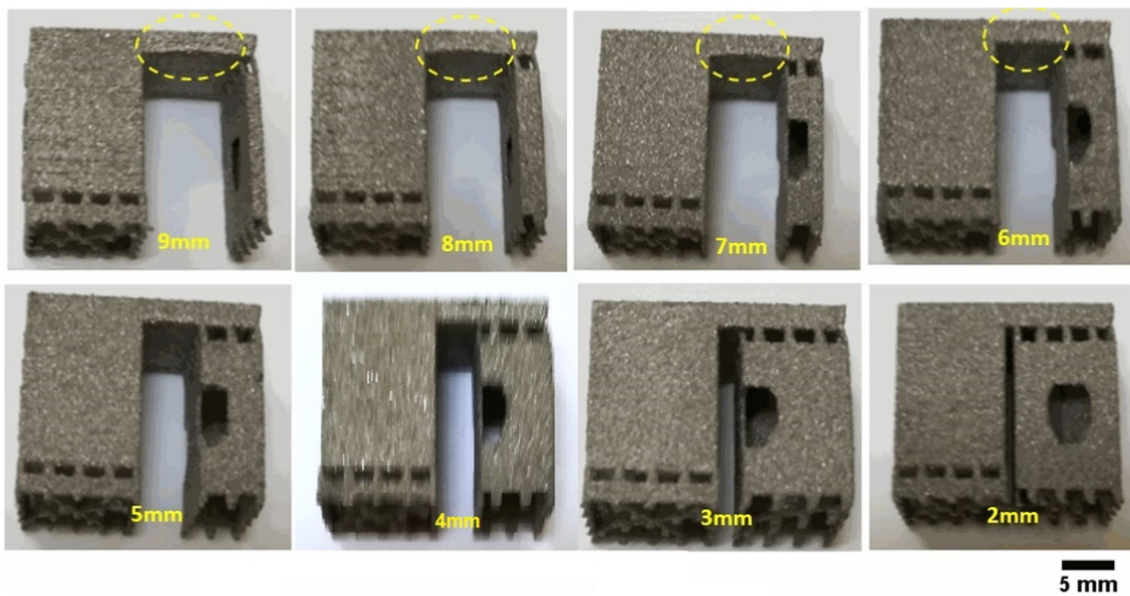


Fig. 30 Segmentation strategy in *X*-direction

Applying the segmentation strategy in the *X*-direction in the middle of the overhang with varying segmentation dimensions, as shown in Fig. 29, showed no change in the warping magnitude and position.

Application of the segmentation strategy in the *X*-direction away from the solid support side resulted in overhangs with lesser deformations. The results indicated the segmentation distance of 5 mm as the limit for defect-free overhangs, as shown in Fig. 30.

The application of this segmentation strategy (5 mm) resulted in reduction of material consumption by 39% and the post-processing time by 57% compared to the specimens produced without segmentation. The segmentation strategy applies supports at an offset from the vertical side surface which prevents the adhesion of the support to the vertical wall. Moreover, the unnecessary supports generated by Magics®

software affect the quality of both overhanging and vertical side surfaces.

3.4 Mechanical properties and microstructures

3.4.1 Microhardness

To see the effect of the overhang geometry on hardness, Vickers microhardness tests were carried out near the edges of the overhangs. Figure 31 shows the hardness results for the self-supporting overhangs. It was found that the hardness values of the convex and slope overhangs were in range of the base material whereas that of the concave overhang was found to be significantly lower as compared to other overhangs.

Fig. 31 Hardness results for self-supporting structures

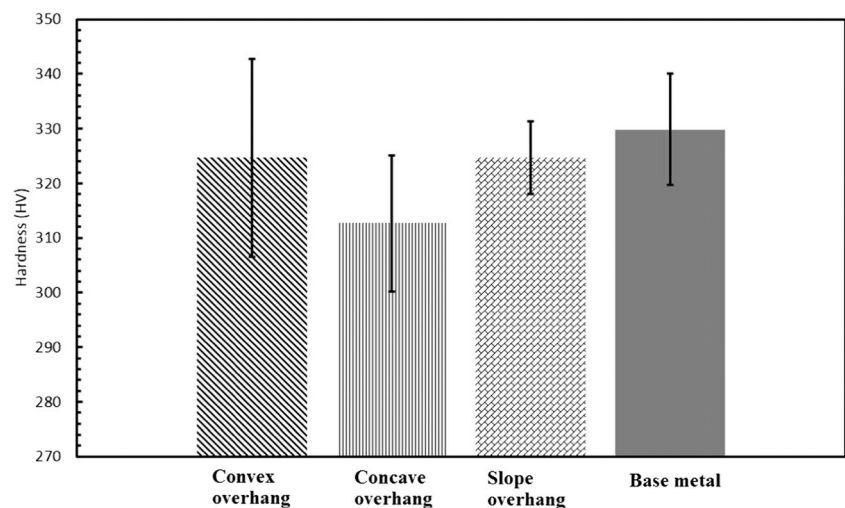
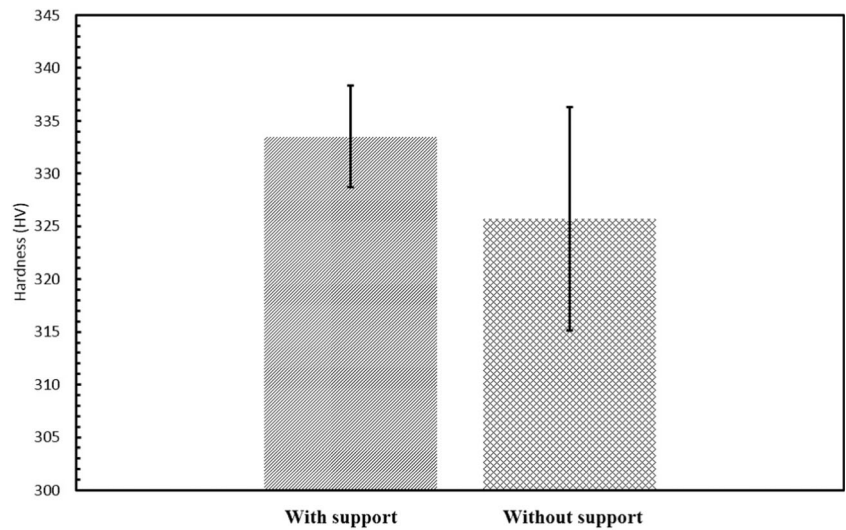


Fig. 32 Effect on support structure on hardness of ledge overhang



To study the effect of the support structure addition on the hardness of the overhangs, Vicker’s microhardness tests were carried out for the ledge overhangs built with support and without support. As shown in Fig. 32, the hardness of the ledge overhang built without support was lower than the overhang built with support. This is because the absence of support structures induces extensive thermal gradients during the

fabrication of ledge overhangs, which in turn affect the microstructure and hardness of the overhang region.

3.4.2 Microstructure

A microstructural analysis of the overhang structures was carried out using optical microscopic images. The microstructures

Fig. 33 Optical microscope images depicting the microstructures. **a** Fully supported edge. **b** Convex overhang edge. **c** Concave edge. **d** Slope overhang edge

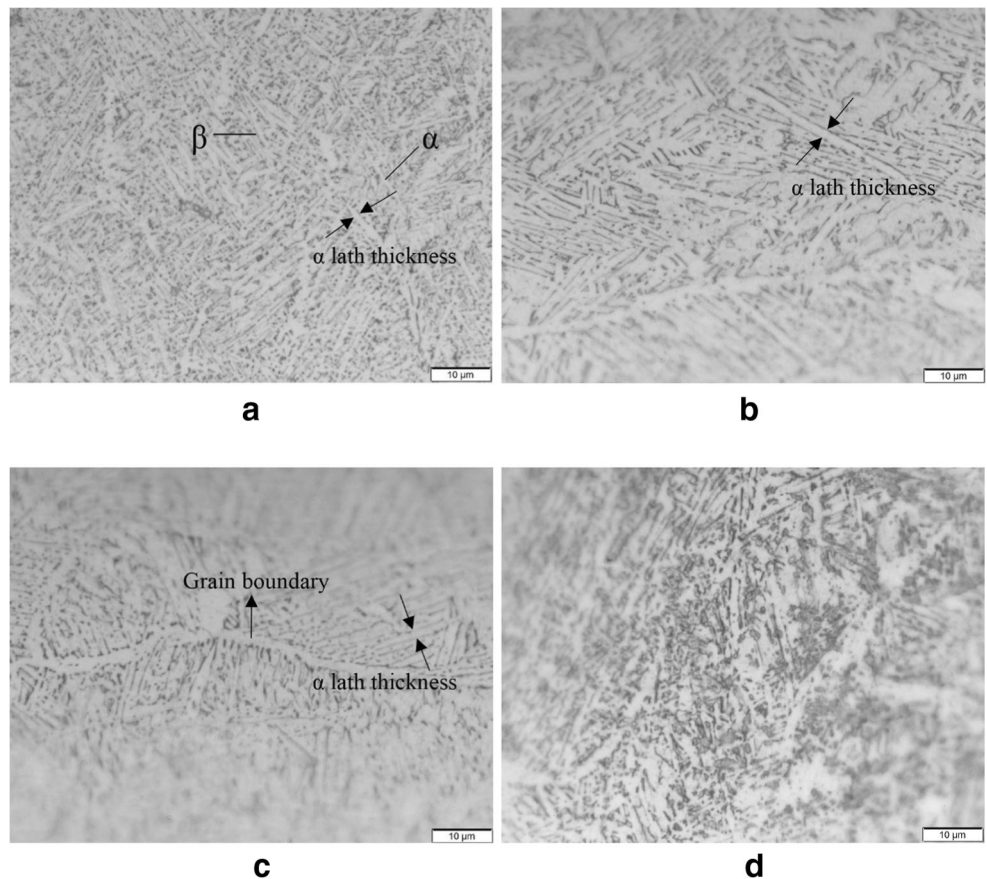
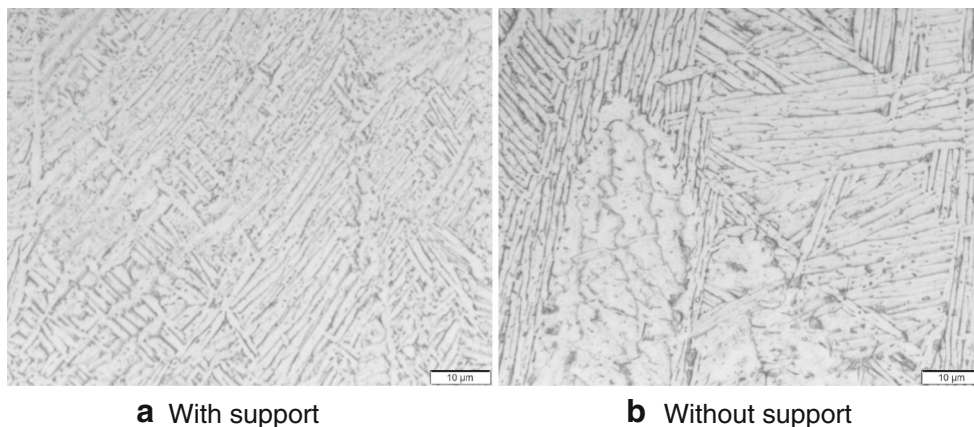


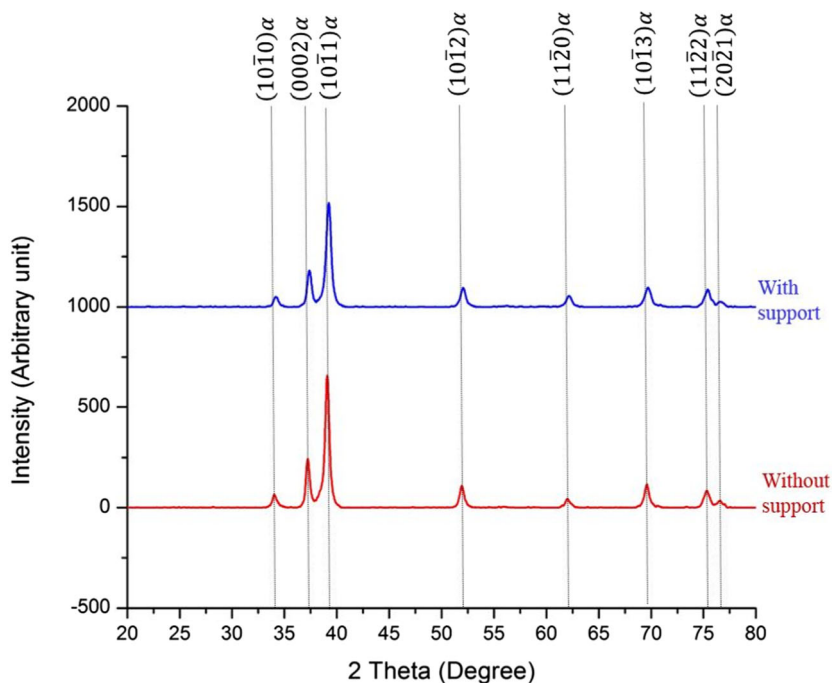
Fig. 34 Optical microscope images depicting the microstructures of the ledge overhang. **a** With support. **b** Without support



near the edges of the different overhang geometries were compared with the fully supported edge of the built part. All the edges showed the Widmanstätten pattern microstructure with approximately the same grain size. However, the α lath thickness was slightly higher for the overhang edges as compared to the fully supported edge, as shown in Fig. 33. This is because the absence of support structures in the overhangs reduces the heat transfer from the top layer to the bottom of the build resulting in thermal gradient and increase in α lath thickness.

The microstructural analysis of the ledge overhangs built with support and without support revealed similar microstructures, with approximately the same grain size. However, the average α lath thickness in the overhang built without support was approximately $1.45 \mu\text{m}$ as compared to $1.02 \mu\text{m}$ in the overhang built with support, as shown in Fig. 34. This increase in the α lath thickness resulted in a decrease in the hardness of the overhang built without support.

Fig. 35 XRD peaks for the ledge overhangs built with and without support



3.4.3 X-ray diffraction peak analysis

The XRD peak analysis was carried out for the ledge overhang samples built with and without support. A similar pattern was observed for the both the ledge overhangs. However, there was a slight shift of the peaks toward the higher angle in case of the overhang built with the support structure, as shown in Fig. 35. This can be attributed to the additional heat and internal stresses in the overhangs built with support structures.

4 Conclusion

This paper presented an overview on the production of Ti6Al4V overhanging structures through EBM. Self-supporting limits of various overhang structures were

established and overhang structures were evaluated. Overhangs with downward-facing surfaces such as convex, concave, slope, ledge, and bridge were considered fundamental overhangs wherein the part deformation was caused by the thermal stresses. The effect of ledge overhang dimensions on the deformation was investigated. Finally, the segmentation strategy for the supports was proposed to reduce the material consumption and the process time.

The following inferences were drawn based on the present study:

- Convex overhangs up to a 7-mm radius can be built without support structures. The fabrication of convex overhangs of more than 7-mm radius without support structures results in shape distortion.
- Concave overhangs up to an 8-mm radius can be built without support structures. The fabrication of concave overhangs of more than 8 mm in radius without support structures results in bottom edge defects and warping.
- Slope overhangs up to 50° edge can be built without support structures. The fabrication of slope overhangs less than 50° without support structures results in wastage of material at the bottom surface.
- Support structures are essential for building ledge overhangs and no self-supporting limit was found for this overhang geometry.
- Bridge overhangs up to 5 mm in length can be built without support structures. The fabrication of bridge overhangs more than 5 mm long without support structures results in warping deformation in the middle portion.
- In case of ledge overhang, as the overhang thickness and width increases, the residual stress increases cumulatively, thereby causing significant warping deformation. However, the deformation decreases as the solid support height of the overhang increases. There was no effect of solid support length on the extent of warping.
- Finally, applying the segmentation strategy in the *X*-direction (near to solid support) with 5-mm dimension gave favorable results in terms of material consumption and the part quality.

The results obtained in this work can be generalized for Ti6Al4V overhangs fabricated by using default process parameters in EBM. This study can further be extended to investigate the effect of process parameters on overhang fabrication.

Acknowledgments The authors thank the Deanship of Scientific Research and RSSU at King Saud University for their technical support.

Funding information This study received funding from the Raytheon Chair for Systems Engineering. The authors are grateful to the Raytheon Chair for Systems Engineering for funding.

References

1. Murr L, Quinones S, Gaytan S, Lopez M, Rodela A, Martinez E et al (2009) Microstructure and mechanical behavior of Ti-6Al-4V produced by rapid-layer manufacturing, for biomedical applications. *J Mech Behav Biomed Mater* 2:20–32
2. Liska WD, Marcellin-Little DJ, Eskelinen EV, Sidebotham CG, Harrysson OL, Hielm-Björkman AK (2007) Custom total knee replacement in a dog with femoral condylar bone loss. *Vet Surg* 36:293–301
3. Moiduddin K, Darwish S, Al-Ahmari A, ElWatidy S, Mohammad A, Ameen W (2017) Structural and mechanical characterization of custom design cranial implant created using additive manufacturing. *Electron J Biotechnol* 29:22–31
4. Murr LE, Gaytan S, Ceylan A, Martinez E, Martinez J, Hernandez D et al (2010) Characterization of titanium aluminide alloy components fabricated by additive manufacturing using electron beam melting. *Acta Mater* 58:1887–1894
5. Poyraz Ö, Akbulut G, Orhangül A, Pilatin S (2015) Investigation of support structures for direct metal laser sintering (DMLS) OF IN625 PARTS. *International Solid Freeform Fabrication Symposium, Austin*
6. Ameen W, Al-Ahmari A, Mohammed MK, Mian SH (2018) Manufacturability of overhanging holes using electron beam melting. *Metals* 8
7. Gan M, Wong C (2016) Practical support structures for selective laser melting. *J Mater Process Technol* 238:474–484
8. Hussein A, Yan C, Everson R, Hao L (2011) Preliminary investigation on cellular support structures using SLM process. *Innovative Developments in Virtual and Physical Prototyping*. Taylor & Francis Group, London, pp 609–612
9. Zeng K. Optimization of support structures for selective laser melting: University of Louisville; 2015.
10. Cheng B, Lu P, Chou K (2014) Thermomechanical investigation of overhang fabrications In *Electron Beam Additive Manufacturing*. ASME 2014 International Manufacturing Science and Engineering Conference collocated with the JSME 2014 International Conference on Materials and Processing and the 42nd North American Manufacturing Research Conference: American Society of Mechanical Engineers, p. V002T02A24–VT02A24
11. Vayre B, Vignat F, Villeneuve F (2013) Identification on some design key parameters for additive manufacturing: application on electron beam melting. *Proc CIRP* 7:264–269
12. Vora P, Derguti F, Mumtaz K, Todd I, Hopkinson N (2013) Investigating a semi-solid processing technique using metal powder bed additive manufacturing processes. *24th Annual International Solid Freeform Fabrication Symposium-An Additive Manufacturing Conference*, Austin, TX, USA
13. Cloots M, Spierings A, Wegener K (2013) Assessing new support minimizing strategies for the additive manufacturing technology SLM. *Proceedings of the Solid Freeform Fabrication Symposium*, Austin, TX, USA, p. 12–3
14. Gan Z, Liu H, Li S, He X, Yu G (2017) Modeling of thermal behavior and mass transport in multi-layer laser additive manufacturing of Ni-based alloy on cast iron. *Int J Heat Mass Transf* 111:709–722
15. Gan Z, Yu G, He X, Li S (2017) Surface-active element transport and its effect on liquid metal flow in laser-assisted additive manufacturing. *Int Commun Heat Mass Transfer* 86:206–214
16. Gan Z, Yu G, He X, Li S (2017) Numerical simulation of thermal behavior and multicomponent mass transfer in direct laser deposition of Co-base alloy on steel. *Int J Heat Mass Transf* 104:28–38
17. Cheng B, Chou K (2014) Thermal stresses associated with part overhang geometry in electron beam additive manufacturing: process parameter effects. *25th Annual International Solid Freeform*

- Fabrication Symposium-An Additive Manufacturing Conference, Austin, TX, USA
18. Cheng B, Chou K (2015) Geometric consideration of support structures in part overhang fabrications by electron beam additive manufacturing. *Comput Aided Des* 69:102–111
 19. Chou Y-S, Cooper K (2014) Systems and methods for designing and fabricating contact-free support structures for overhang geometries of parts in powder-bed metal additive manufacturing. Google Patents
 20. RamiTounsi FV (2017) New concept of support structures in electron beam melting manufacturing to reduce geometric defects. 15e Colloque National AIP-Priméca
 21. Cheng B, Chou YK (2017) Overhang Support structure design for electron beam additive manufacturing. ASME 2017 12th International Manufacturing Science and Engineering Conference collocated with the JSME/ASME 2017 6th International Conference on Materials and Processing: American Society of Mechanical Engineers. p. V002T01A18–VT01A18
 22. Calignano F, Manfredi D (2013) Production of overhanging structures by DMLS. High value manufacturing: advanced research in virtual and rapid prototyping: Proceedings of the 6th International Conference on Advanced Research in Virtual and Rapid Prototyping, Leiria, Portugal, 1-5 October, 2013. CRC Press, p. 61
 23. Thomas D (2009) The development of design rules for selective laser melting: University of Wales
 24. Cheng B, Chou K (2015) Deformation evaluation of part overhang configurations in electron beam additive manufacturing. ASME 2015 International Manufacturing Science and Engineering Conference: American Society of Mechanical Engineers. p. V001T02A72–VT02A72
 25. Calignano F (2014) Design optimization of supports for overhanging structures in aluminum and titanium alloys by selective laser melting. *Mater Des* 64:203–213
 26. Mohammad A, Al-Ahmari AM, AlFaify A, Mohammed MK (2017) Effect of melt parameters on density and surface roughness in electron beam melting of gamma titanium aluminide alloy. *Rapid Prototyp J* 23:474–485

Publisher's note Springer Nature remains neutral with regard to jurisdictional claims in published maps and institutional affiliations.